ISSN 0031-918X, Physics of Metals and Metallography, 2023. © Pleiades Publishing, Ltd., 2023.

STRUCTURE, PHASE TRANSFORMATIONS, AND DIFFUSION

Auger Electron Spectroscopy of Thin Cr_2GeC Films

T. A. Andryushchenko[a], *, S. A. Lyaschenko[a], S. N. Varnakov[a], A. V. Lukyanenko[a], I. V. Nemtsev[a], I. A. Yakovlev[a], D. V. Shevtsov[a], O. A. Maximova[a], and S. G. Ovchinnikov[a]

[a] *Kirensky Institute of Physics, Federal Research Center KSC SB RAS, Krasnoyarsk, 660036 Russia*

**e-mail: ata12@iph.krasn.ru*

Received July 30, 2023; revised September 4, 2023; accepted September 19, 2023

Abstract—Auger electron spectroscopy was used to determine the phase composition of Cr_2GeC MAX phase thin films. A distinctive feature of the formation of carbon-containing MAX phases is the shape of carbon Auger peaks, which is characteristic of metal carbides spectra. Features of the Auger spectra in the presence of secondary phases of chromium germanides are found. Their presence can manifest itself in an increase in the energy of the germanium peaks, which is caused by a chemical shift during the formation of the Cr–Ge bond. Moreover, we have detected the accumulation of electronic charge, which can be explained by the features of the surface morphology.

Keywords: MAX phases, chromium germanides, epitaxial thin films, Auger electron spectroscopy, magnetron sputtering co-deposition

DOI: 10.1134/S0031918X2360135X

INTRODUCTION

MAX phases are nanolayered hexagonal carbides or nitrides of transition metals, alternating with layers of an A-element (mainly 13–15 groups of the periodic table) with the general formula $M_{n+1}AX_n$ (where n = 1–4, M is a transition metal, X is carbon or nitrogen). Due to their layered structure, where the M-X layers have strong covalent bonds and the M–A layers have weaker ionic bonds, MAX phases have the properties of ceramic materials (such as thermal stability, oxidation resistance [1–3]) and high thermal- and electrical conductivity characteristic of metals. The layering of the MAX phases also manifests itself in the anisotropy of properties along different directions. Furthermore, the compounds can exhibit superconductivity [4, 5], ferromagnetism, and antiferromagnetism [6–8] depending on the combination of elements used.

Studies of manganese and iron doped Cr_2GeC MAX phases demonstrate that an epitaxial $(Cr_{0.75}Mn_{0.25})_2GeC$ thin film [9] is a non-collinear antiferromagnetic with a magnetic signal at room temperature, and ferromagnetic bulk samples of $(Cr_{0.8}Mn_{0.2})_2GeC$ [10] and $(Cr_{0.95}Fe_{0.05})_2GeC$ [11] have FM–PM transition temperatures of 270 and 390 K, respectively. This shows the relevance of these structures for applications in spintronics and magnonics. To obtain compounds of this type in the form of epitaxial thin films using sputtering techniques, it is expedient to switch from the ternary Cr_2GeC to quaternary MAX phase synthesis technology with the replacement of chromium with other elements by varying the technological conditions of synthesis. In the process of synthesizing doped quaternary MAX films, it is important to control the preservation of the phase composition of the samples. One of the effective in situ methods for controlling the phase composition of epitaxial thin films is electron diffraction. However, due to the similarity of electron diffraction patterns of Cr_2GeC and chromium germanides (Fig. 1), which are formed in case of a lack of carbon, confirmation of the phase composition of MAX phase thin films is difficult. This requires the use of an additional phase

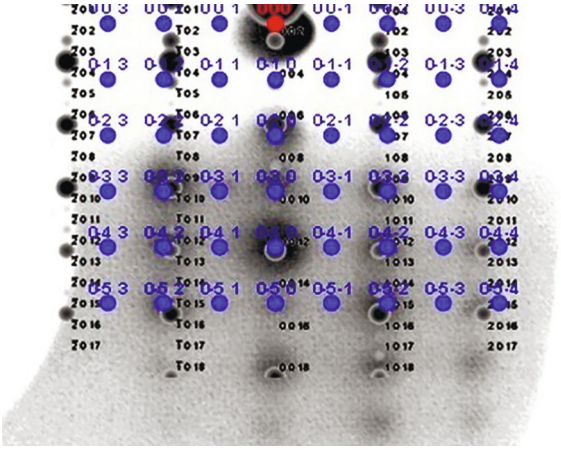

Fig. 1. Diffraction patterns for Cr_2GeC [100] (gray and black dots) and CrGe [100] (blue dots) calculated within the framework of the kinematic theory of diffraction superimposed on the experimental Cr_2GeC XRD pattern.

Table 1. Synthesis parameters, phase and elemental composition, morphology of Cr_2GeC thin films

Sample number	Thickness, nm	Technological atomic concentrations, %			Phase composition by XRD	Morphology (shape, diameter D, height h, length L of crystallites, tilt angle φ between rods or bars, multiplicity factor N) and root-mean-square roughness S_q by AFM	Cr/Ge atomic ratio by XRF
		Cr	Ge	C			
1	10	49.7	25.6	24.6	–	Spherical grains D_g = 20–50 nm, h_g = 4.28 ± 0.64 nm; S_q = 1.024 nm	1.66 ± 0.40
2		50	25.2	24.8	–	Spherical grains D_g = 15–45 nm, h_g = 5.64 ± 0.30 nm; S_q = 1.549 nm	1.92 ± 0.58
3		50.1	19.7	30.2	–	Spherical grains D_g = 20–50 nm, h_g = 13.37 ± 1.97 nm; S_q = 3.110 nm	2.04 ± 0.52
4		54.4	20.3	25.3	Cr_3Ge(002)	Spherical grains D_g = 20–70 nm, h_g = 8.52 ± 1.46 nm; S_q = 2.304 nm	7.47 ± 2.38
5	40	54.4	20.3	25.3	Cr_2GeC(00L) CrGe(012) Cr_2GeC(013)	Spherical grains D_g = 15–30 nm; Rods L_r = 100–150 nm, D_r = 40–100 nm, $\varphi_r = N \times 30°$; h_g = 1–1.5 nm; S_q = 4.031 nm	1.88 ± 0.31
6	100	54.4	20.3	25.3	Cr_2GeC(00L) CrGe(012) Cr_2GeC(013)	Incline plates D_p = 100–300 nm, h_p = 30 nm; bars L_b = 100–150 nm, D_b = 40–100 nm, $\varphi_b = N \times 30°$; S_q = 8.553 nm	1.47 ± 0.22
7	40.6	55	16.8	28.2	Cr_3Ge(002) CrGe(012) Cr_2GeC(013)	Elongated grains D_g = 40–100 nm, h_g = 4–12 nm; S_q = 9.329 nm	2.17 ± 0.41
8	40	55	16.8	28.2	Cr_2GeC(00L) Cr_2GeC(013)	Elongated grains D_g = 40–90 nm, h_g = 2–20 nm; S_q = 8.490 nm	2.59 ± 0.48

composition in situ control technique with exclusion of the atmosphere effect. Auger electron spectroscopy (AES) can be such a method. With its help, it is possible not only to determine the elemental composition of the surface layers of thin films, but also to identify chemical bonds according to the shape of peaks or chemical shifts [12]. Thus, the purpose of this work was to reveal the features of the Auger electron spectra of synthesized samples of ternary Cr_2GeC MAX phase epitaxial thin films on MgO (111) substrates.

EXPERIMENTAL

Synthesis of Cr_2GeC thin films was carried out on the ultrahigh vacuum (UHV) setup at the Magnetic MAX materials laboratory in the Kirensky Institute of Physics SB RAS (created under Megagrant project (agreement no. 075-15-2019-1886) using magnetron sputtering co-deposition. Cr (99.95%) and C (99.95%) targets were sputtered in DC-mode, Ge (99.99%) in RF-mode with argon flow (99.99995%) of 10 sccm and a pressure of about 0.933 Pa. The deposition of thin films with technological thicknesses of 10, 40, 40.6, and 100 nm was performed on MgO (111) substrates preliminarily cleaned using Ar-ion etching and heated to 820 ± 20°C. After deposition, the samples were annealed in UHV at a base pressure of 1.33×10^{-6} Pa.

The deposition of thin Cr_2GeC films of samples *1–8* was carried out at various technological concentrations of chromium, germanium, and carbon, which are presented in Table 1. More detailed information on the synthesis process, morphology, optical and transport properties of the thin Cr_2GeC films is presented in [13].

A low energy diffraction and Auger electron analysis system ErLEED 100 (SPECS, Germany) was used to record AES spectra. The primary electron energy was 2500 eV, electron beam diameter was <1 mm, electron emission current and accelerating voltage were ~0.4 μA and 550 V, respectively. Electrons were incident along the normal to the surface. The spectrum recording step was 0.2 eV, the approximate recording time was the same for all spectra and was about 1 h (500 ms for each point of the spectrum). The

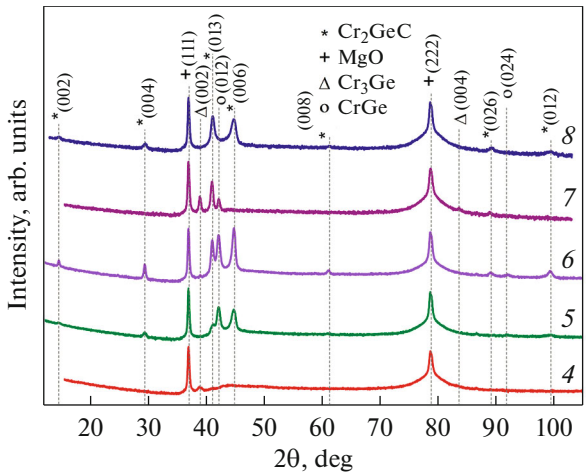

Fig. 2. The XRD patterns of samples *4–8*.

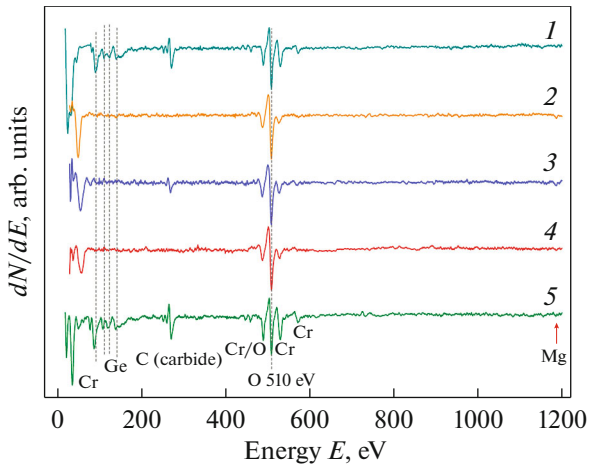

Fig. 3. The Auger spectra of samples *1–5*.

root-mean-square deviation of Auger peak energy measurements was no more than 0.5 eV. The spectrometer was preliminarily calibrated on a clean MgO (111) substrate and separate thin 50 nm films of chromium, germanium, and carbon, obtained by the magnetron deposition technique from the same targets as the samples under study.

Structure characterization was performed by X-ray diffraction (XRD) analysis using PANalytical X'Pert PRO diffractometer equipped with a solid state detector PIXcel on Cu$K\alpha$ radiation. The XRD patterns of samples *4–8* are shown in Fig. 2.

Film morphology was studied by atomic force microscopy (AFM) in tapping mode using NanoInk DPN 5000 instrument. The roughness analysis of the AFM data was carried out with Gwyddion software.

Elemental analysis and determination of the Cr/Ge atomic ratio were performed using X-ray fluorescence (XRF) analysis. The integral intensities of the characteristic lines Cr$K\alpha_1$, Cr$K\alpha_2$ and Ge$K\alpha_1$ were calculated using the approximation of the calibration spectra of chromium and germanium thin films by Gaussian curves.

The electron micrographs were obtained using a Hitachi SU3500 scanning electron microscope at a magnification of 25 thousand times.

RESULTS AND DISCUSSION

The differential Auger electron spectra of the surfaces of samples *1–8* are shown in Figs. 3, 4, and 5. A common feature of all spectra is the presence of the Auger signal from the substrate, which is displayed as an oxygen Auger peak with energies of about 510 eV and magnesium Auger peaks with sample-averaged energies of 32.2 and 1186.0 eV. This is indicative of island morphology of the thin films, as confirmed by AFM data and scanning electron microscopy data (Fig. 6, light gray islands against a dark gray substrate). To eliminate the effect of sample oxidation, we checked the time stability of oxygen peaks in samples under UHV conditions during the day. The presence of chemical shifts of the Auger peaks characteristic of the formation of a bond with oxygen [12] was not recorded. The morphology of the films according to AFM data differs between the samples, it is mainly represented by spherical and elongated grains, rods and incline plates (Table 1).

A signature of the formation of carbon-containing MAX phases is the formation of layers with a bond between carbon and a transition metal, in our case, chromium. On the Auger spectra, the peaks of carbon (including carbides) in the *M–C* bond appear as a characteristic set of three peaks in the energy range of 245–280 eV [14–17]. The spectra of samples *1*, *3*, and *5* (Fig. 3) show these peaks, with the most intense peak located at 271.5 eV. There are no carbon peaks in the

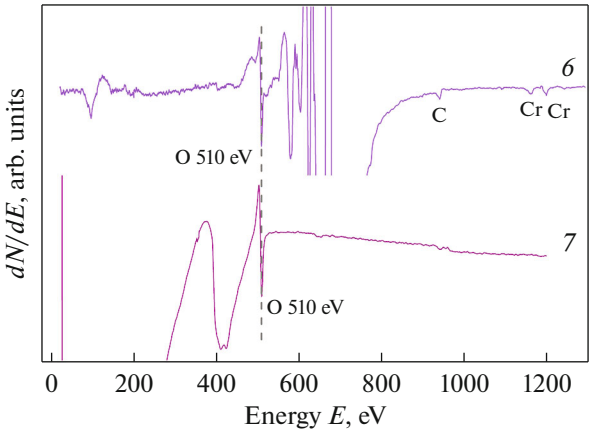

Fig. 4. Distorted due to the accumulation of electronic charge Auger spectra of samples *6* and *7*.

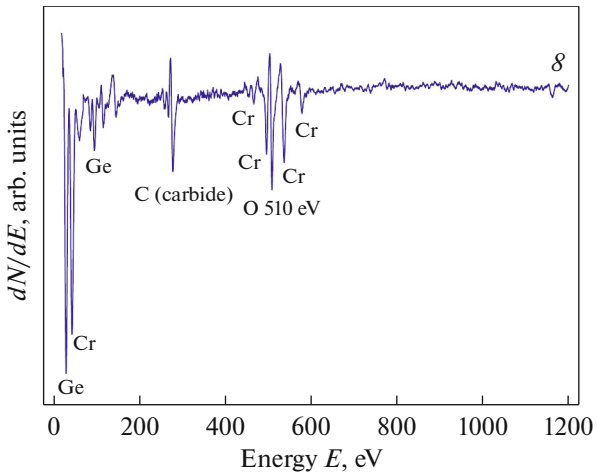

Fig. 5. Auger spectrum of sample *8* with a peak shift of +(7 ± 1) eV.

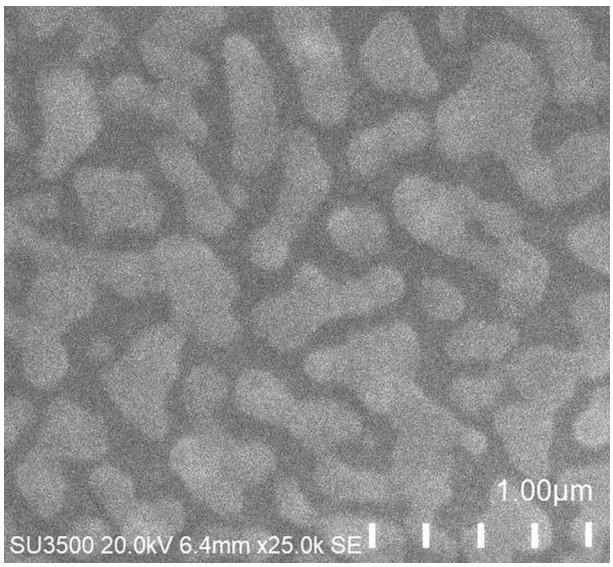

Fig. 6. The scanning electron micrograph of sample *6*.

Auger spectra of samples *2* and *4*, which is explained by the formation of chromium germanide according to the results of XRD analysis of sample *4*, as well as by similar synthesis conditions for both samples (technological atomic concentration of carbon 24.8 and 25.3%, respectively). We carried out the selection of technological stoichiometry for the synthesis of subsequent samples, taking into account the need for the appearance of Cr–C bond carbon Auger peaks in the spectra.

In the energy range of 45–180 eV, the Auger peaks of germanium are shifted by +(3.0 ± 0.4) eV in the spectrum of sample *1* compared to the spectrum of sample *5*. The increase in the energy of germanium Auger peaks in the spectrum of sample *1* can be explained by a chemical shift in the chromium germanide compound.

To interpret the observed chemical shifts, one can estimate the changes in the Auger electron kinetic energy E_A, described by the formula:

$$E_A = E_B - E_C - E_D - U(C, D) - \varphi, \qquad (1)$$

where E_B, E_C, and E_D are the ionization energies (B, C, and D are the designations for transitions between electronic levels K, L, M, etc.), $U(C, D)$ is a term that takes into account the double ionization of an atom as a result of the formation of vacancies, and φ is the work function of an electron [18]. An increase in the kinetic energy of the Auger electron can manifest itself as a result of a decrease in the electron binding energy at the E_C level, where the formation of a secondary vacancy of the Auger process, and the Auger electron yield level E_D.

According to the photoelectron spectra from [19], the formation of the Cr–Ge bond is characterized by a decrease in the binding energy of electrons with the nucleus at the *3d*-levels of germanium atoms compared to the Ge–Ge bond. The change in the binding energy of electrons in chromium atoms in the case of the Cr–Ge bond is less than 0.5 eV, which is commensurate with the error of our measurements.

We exclude the possibility of the formation of germanium carbides, since their formation, according to [20], is accompanied by an increase in the binding energy of the Ge $2p_{3/2}$ line, and, accordingly, a decrease in the kinetic energy of germanium Auger peaks, which does not correspond to the behavior observed in the spectrum of sample *1*.

Based on the described differences between the Auger spectra of samples *1* and *5*, it can be concluded that there is a presence and a higher content of chromium germanides in the composition of thin film *1* compared to *5*. It is confirmed by calculations of the Cr/Ge atomic ratio based on XRF data: 1.66 ± 0.40 for sample *1* and 1.88 ± 0.31 for sample *5*.

A feature of samples *6* and *7* was the presence of distortions in the Auger spectra (Fig. 4) caused by the appearance of a negative surface potential due to the accumulation of an electronic charge by the surface of the samples [21–23]. A distinct peak with an energy of 510 eV can be interpreted as an Auger peak of oxygen from the substrate. There is no peak shift, and this is explained by the release of Auger electrons from atoms in that part of the sample where charge does not accumulate [24]. Such areas are the not covered by a thin film areas of the magnesium oxide dielectric substrate, which has a zero surface potential due to the balance between oppositely charged layers during electron irradiation [22].

All phases in films *6*, *7*, and *8* are conductive [25–27], and the conduction paths of island films are preferentially through the substrate rather than tun-

neling because of great distances between particles [28, 29]. With such a conduction mechanism, electrons can get stuck on trapping centers, which form at the film/substrate interface in the form of electronic levels of film atoms located in the energy band gap of MgO [21, 23]. As thin films grow, the islands increase in size, and they can be considered as extended isolated conduction bands, where secondary or primary electrons after inelastic collisions can be retained.

The accumulation of a surface charge makes it difficult to interpret the Auger spectra of samples *6* and *7*. However, the spectrum of thin film *6* contains peaks with values of 941.1, 1161.8, 1200.0, and 1243.5 eV, which, in terms of energy differences between the peaks, coincide with the peaks of carbon and chromium with average energies of 271.3, 489.0, 529.4, and 572.0 eV in the spectra of samples *1*–*5*. If we assume that these peaks are interpreted as Auger peaks of carbon and chromium shifted due to the accumulation of electron charge [20], then the surface potential is about –670 V. In the spectrum of sample *7* such peaks are absent which may indicate their location outside our detection region due to a negative surface potential of more than 930 V. A decrease in the primary electron current density and an increase in the secondary electron emission coefficient δ (by reducing the primary electron energy up to 1000 eV) [30, 31] did not affect the value of the surface potential.

Analysis of the Auger spectrum of sample *8* (Fig. 5), where the phase composition of the thin film is represented exclusively by the MAX phase of Cr_2GeC, shows the presence of Auger peaks of chromium, germanium, carbon in the form of carbide, which corresponds to the elemental composition of the synthesized compound. However, this spectrum also shows a shift of all peaks of a thin film due to the accumulation of electron charge, but the shift value is $+(7 \pm 1)$ eV relative to the peak positions of the calibration samples. Despite the fact that the values of chemical shifts can be comparable with this value [32], such an explanation is not suitable due to the same shift of all Auger peaks of the thin film.

The existing differences in the values of the negative surface potential of samples *6*, *7*, and *8* are not related to the duration of electron irradiation, since the recording time of the spectra of all samples is the same. These differences are the result of a combination of the surface morphology of the samples and their phase composition, since only the surface roughness of the samples (Table 1) is not enough to explain the magnitude of the Auger peak shifts, as, for example, the authors of [33] showed.

CONCLUSIONS

We have shown that Auger electron spectroscopy can be used as a method for monitoring the phase composition of thin MAX films due to the characteristic shape of carbon Auger peaks in the case of Cr–C bonding and the analysis of chemical shifts of germanium Auger peaks during the formation of chromium germanides.

The distortions of the Auger electron spectra caused by the accumulation of an electronic charge can be used to estimate the morphology parameters of epitaxial Cr_2GeC MAX phase thin films on MgO(111) after an additional study on samples of the same phase composition.

ACKNOWLEDGMENTS

The authors thank the Krasnoyarsk Regional Center of Research Equipment of Federal Research Center "Krasnoyarsk Science Center SB RAS" for obtaining the AFM data, X-ray diffraction patterns, scanning electron micrographs and L. A. Solovyov for the help in processing the XRD data.

FUNDING

The research was supported by the Russian Science Foundation (grant no. 21-12-00226, http://rscf.ru/project/21-12-00226/).

CONFLICT OF INTEREST

The authors of this work declare that they have no conflicts of interest.

REFERENCES

1. D. J. Tallman, B. Anasori, and M. W. Barsoum, "A critical review of the oxidation of Ti_2AlC, Ti_2AlC_2 and Cr_2AlC in air," Mater. Res. Lett. **1**, 115–125 (2013). https://doi.org/10.1080/21663831.2013.806364
2. D. Yu and Yo. Tan, "Oxidation behaviors of compositionally complex MAX phases in air," Ceram. Int. **47**, 30188–30193 (2021). https://doi.org/10.1016/j.ceramint.2021.07.198
3. T. S. Mathis, K. Maleski, A. Goad, A. Sarycheva, M. Anayee, A. C. Foucher, K. Hantanasirisakul, C. E. Shuck, E. A. Stach, and Yu. Gogotsi, "Modified MAX phase synthesis for environmentally stable and highly conductive Ti_2C_2 MXene," ACS Nano **15**, 6420–6429 (2021). https://doi.org/10.1021/acsnano.0c08357
4. A. D. Bortolozo, O. H. Sant'Anna, C. A. M. dos Santos, and A. J. S. Machado, "Superconductivity at 9.5 K in the Ti_2GeC compound," Mater. Sci.-Poland **30**, 92–97 (2012). https://doi.org/10.2478/s13536-012-0013-4
5. Z. Babar, J. Fatheema, N. Arif, M. S. Anwar, S. Gul, M. Iqbal, and S. Rizwan, "Magnetic phase transition from paramagnetic in Nb_2AlC-MAX to superconductivity-like diamagnetic in Nb2C-MXene: An experimental and computational analysis," (2020).

6. A. S. Ingason, M. Dahlqvist, and J. Rosen, "Magnetic MAX phases from theory and experiments; a review," J. Phys.: Condens. Matter **28**, 433003 (2016). https://doi.org/10.1088/0953-8984/28/43/433003
7. J. Yang, G. Yao, S. Sun, Z. Chen, S. Yuan, K. Wu, X. Fu, Q. Wang, and W. Cui, "Structural, magnetic properties of in-plane chemically ordered $(Mo_{2/3}R_{1/3})_2AlC$ (R = Gd, Tb, Dy, Ho, Er and Y) MAX phase and enhanced capacitance of $Mo_{1.33}C$ MXene derivatives," Carbon **179**, 104–110 (2021). https://doi.org/10.1016/j.carbon.2021.03.062
8. J. Dey, E. Jedryka, R. Kalvig, U. Wiedwald, M. Farle, J. Rosen, and M. Wójcik, "Helical magnetic structure of epitaxial films of nanolaminated Mn_2GaC MAX phase," Phys. Rev. B **108**, 54413 (2023). https://doi.org/10.1103/physrevb.108.054413
9. A. S. Ingason, A. Mockute, M. Dahlqvist, F. Magnus, S. Olafsson, U. B. Arnalds, B. Alling, I. A. Abrikosov, B. Hjörvarsson, P. O. Å. Persson, and J. Rosen, "Magnetic self-organized atomic laminate from first principles and thin film synthesis," Phys. Rev. Lett. **110**, 195502 (2013). https://doi.org/10.1103/physrevlett.110.195502
10. Z. Liu, T. Waki, Y. Tabata, and H. Nakamura, "Mn-doping-induced itinerant-electron ferromagnetism in Cr_2GeC," Phys. Rev. B **89**, 54435 (2014). https://doi.org/10.1103/physrevb.89.054435
11. S. Lin, Ya. Huang, L. Zu, X. Kan, J. Lin, W. Song, P. Tong, X. Zhu, and Yu. Sun, "Alloying effects on structural, magnetic, and electrical/thermal transport properties in MAX-phase $Cr_{2-x}M_xGeC$ (M = Ti, V, Mn, Fe, and Mo)," J. Alloys Compd. **680**, 452–461 (2016). https://doi.org/10.1016/j.jallcom.2016.04.197
12. D. Briggs and M. P. Seah, *Practical Surface Analysis by Auger and X-ray Photoelectron Spectroscopy* (John Wiley & Sons, Chichester, 1983).
13. A. S. Tarasov, S. A. Lyaschenko, M. V. Rautskii, A. V. Lukyanenko, T. A. Andryushchenko, L. A. Solovyov, I. A. Yakovlev, O. A. Maximova, D. V. Shevtsov, M. A. Bondarev, I. A. Bondarev, S. G. Ovchinnikov, and S. N. Varnakov, "Growth process, structure and electronic properties of Cr_2GeC and $Cr_{2-x}Mn_xGeC$ thin films prepared by magnetron sputtering," Processes **11**, 2236 (2023). https://doi.org/10.3390/pr11082236
14. T. A. Andryushchenko, S. A. Lyaschenko, A. V. Lukyanenko, S. N. Varnakov, and S. G. Ovchinnikov, "Auger electron spectroscopy of the air exposed $(Cr_{0.5}Mn_{0.5})_2GaC$ MAX film surface," PJTF **49** (14), 22–27 (2023). https://doi.org/10.21883/PJTF.2023.14.55821.19430
15. M. A. Smith and L. L. Levenson, "Final-state effects in carbon Auger spectra of transition-metal carbides," Phys. Rev. B **16**, 1365–1369 (1977). https://doi.org/10.1103/physrevb.16.1365
16. S. Danyluk, J. Yu. Park, and D. E. Busch, "Auger electron spectroscopy of stoichiometric chromium carbides and carbide precipitates at grain boundaries of type 304 stainless steel," Scr. Metall. **13**, 857–862 (1979). https://doi.org/10.1016/0036-9748(79)90174-1
17. T. W. Haas, J. T. Grant, and G. J. Dooley, "Chemical effects in Auger electron spectroscopy," J. Appl. Phys. **43**, 1853–1860 (1972). https://doi.org/10.1063/1.1661409
18. C. C. Chang, "Auger electron spectroscopy," Surf. Sci. **25**, 53–79 (1971). https://doi.org/10.1016/0039-6028(71)90210-x
19. M. W. Ruckman, M. Del Giudice, J. J. Joyce, and J. H. Weaver, "Comparative study of the formation of Cr/Ge and Ge/Cr thin-film interfaces," Phys. Rev. B **33**, 8039–8047 (1986). https://doi.org/10.1103/physrevb.33.8039
20. P. Sander, M. Altebockwinkel, W. Storm, L. Wiedmann, and A. Benninghoven, "Surface and in-depth analysis of hydrogenated carbon layers on silicon and germanium by mass and electron spectroscopy," J. Vac. Sci. Technol. B: Microelectron. Process. Phenom. **7**, 517–528 (1989). https://doi.org/10.1116/1.584778
21. P. J. Møller and J. He, "Electron beam induced charging of Cu/MgO surfaces," Nucl. Instrum. Methods Phys. Res., Sect. B: Beam Interact. Mater. Atoms **17**, 137–140 (1986). https://doi.org/10.1016/0168-583x(86)90075-3
22. J. Cazaux, K. H. Kim, O. Jbara, and G. Salace, "Charging effects of MgO under electron bombardment and nonohmic behavior of the induced specimen current," J. Appl. Phys. **70**, 960–965 (1991). https://doi.org/10.1063/1.349606
23. C. C. Chang, *Characterization of Solid Surfaces* (Plenum Press, New York, 1974).
24. H. Guo, W. Maus-Friedrichs, and V. Kempter, "Charging phenomena and charge compensation in AES on metal oxides and silica," Surf. Interface Anal. **25**, 390–396 (1997). https://doi.org/10.1002/(sici)1096-9918(199706)25:6<390::aid-sia247>3.0.co;2-x
25. P. Eklund, M. Bugnet, V. Mauchamp, S. Dubois, C. Tromas, J. Jensen, L. Piraux, L. Gence, M. Jaouen, and T. Cabioc'h, "Epitaxial growth and electrical transport properties of Cr_2GeC thin films," Phys. Rev. B **84**, 75424 (2011). https://doi.org/10.1103/physrevb.84.075424
26. N. Lundberg, M. Östling, and F. M. D'Heurle, "Chromium germanides: Formation, structure and properties," Appl. Surf. Sci. **53**, 126–131 (1991). https://doi.org/10.1016/0169-4332(91)90252-f
27. T. Chihi, M. Fatmi, and M. A. Ghebouli, "Ab initio study of some fundamental properties of the M_3X (M = Cr, V; X = Si, Ge) compounds," Phys. B: Condens. Matter **407**, 3591–3595 (2012). https://doi.org/10.1016/j.physb.2012.05.032
28. R. M. Hill, "Electrical conduction in ultra thin metal films I. Theoretical," Proc. R. Soc. London A: Math. Phys. Sci. **309**, 377–395 (1969). https://doi.org/10.1098/rspa.1969.0048
29. E. V. Vashchenko, I. A. Gladskikh, S. G. Przhibel'skiĭ, V. V. Khromov, and T. A. Vartanyan, "Conductivity and photoconductivity of granular silver films on a sap-

phire substrate," J. Opt. Technol. **80**, 263 (2013). https://doi.org/10.1364/jot.80.000263

30. S. Hofmann, "Charging and charge compensation in AES analysis of insulators," J. Electron Spectrosc. Relat. Phenom. **59**, 15–32 (1992). https://doi.org/10.1016/0368-2048(92)85009-v

31. C. G. H. Walker, M. M. El-gomati, A. M. D. Assa'd, and M. Zadražil, "The secondary electron emission yield for 24 solid elements excited by primary electrons in the range 250–5000 eV: A theory/experiment comparison," Scanning **30**, 365–380 (2008). https://doi.org/10.1002/sca.20124

32. H. H. Madden, "Chemical information from Auger electron spectroscopy," J. Vac. Sci. Technol. **18**, 677–689 (1981). https://doi.org/10.1116/1.570927

33. J.-W. Park, "Sample charging of insulators with rough surfaces during Auger electron spectroscopy analysis," J. Vac. Sci. Technol. A: Vac., Surf., Films **15**, 292–293 (1997). https://doi.org/10.1116/1.580527